LOW SPEED WIND TUNNEL INVESTIGATION OF PROPELLER SLIPSTREAM AERODYNAMIC EFFECTS ON DIFFERENT NACELLE/WING COMBINATIONS

ICAS-88-4.11.1

by
Ingemar Samuelsson
The Aeronautical Research Institute of Sweden (FFA),
Box 11021, S-161 11 BROMMA, Sweden

Abstract

A low speed wind tunnel investigation of propeller slipstream/nacelle/wing aerodynamic interference effects has been carried out for four nacelle/wing combinations. Detailed nacelle and wing surface pressures were obtained by means of the Scanivalve technique. The test was performed with different angles of attack and yaw, freestream speeds and thrust coefficients.

For three of the configurations also the propeller slipstream flow fields were surveyed by means of a five-hole pressure probe traversed along radial lines. Some of the obtained slipstream flow results are shown in the paper (3D velocity and static pressure).

The experimental data show that there are significant propeller slipstream induced lateral nacelle loads (side force, yawing moment and rolling moment). A propeller set at incidence experiences a cyclic thrust variation on its individual blades, thereby creating an asymmetrical slipstream pressure field. When this asymmetrical slipstream washes the nacelle surfaces there will be lateral loads acting on the nacelle. For a non-axisymmetrical ("high") nacelle lateral nacelle loads develop even at zero incidence and zero yaw, due to interference between the propeller slipstream pressure field and the nacelle surfaces. There are also significant effects of the thrust coefficient C_F on the development of the lateral nacelle loads.

Nomenclature

A	aspect ratio of wing = (wing span)^2/wing area	
b	wing span	[m]
c	wing chord	[m]
C_F	propeller thrust coefficient	$= T/q_\infty S$
C_ℓ	rolling moment coefficient	$= \ell/q_\infty S\ c$
C_m	pitching moment coefficient	$= m/q_\infty S\ c$
C_n	yawing moment coefficient	$= n/q_\infty S\ c$
C_p	pressure coefficient	$= (p-p_\infty)/q_\infty$
C_P	propeller power coefficient	$= P/\rho_\infty N^3 D^5$
C_T	propeller thrust coefficient	$= T/\rho_\infty N^2 D^4$
C_X	tangential force coefficient	$= X/q_\infty S$
C_Y	side force coefficient	$= Y/q_\infty S$
C_Z	normal force coefficient	$= Z/q_\infty S$
D	propeller diameter	[m]
J	advance ratio	$= U_\infty/(ND)$
ℓ	rolling moment	[Nm]
m	pitching moment	[Nm]
n	yawing moment	[Nm]
N	propeller rotational speed	[rev/s]
p	static pressure	[Pa]
P	propeller shaft power = $Q\omega$	[W]
q_∞	freestream dynamic pressure = $1/2\ \rho_\infty U_\infty^2$	[Pa]
Q	propeller shaft torque	[Nm]
r	radius	[m]
R_p	propeller radius = D/2	[m]
S	reference area	[m^2]
T	propeller thrust	[N]
U	flow velocity	[m/s]
x,y,z	nacelle fixed coordinate system	[m]
X	tangential force	[N]
Y	side force	[N]
Z	normal force	[N]
α	angle of attack	[°]
β	angle of yaw	[°]
$\beta_{.75}$	propeller blade angle at 75% propeller radius (measured relatively propeller disk plane)	[°]
η	propeller efficiency = $T\ U_\infty/P$	
ω	propeller shaft angular speed = $2\pi N$	[rad/s]
ρ	air density	[kg/m^3]
ϕ	angular position	[°]

Subscripts

∞	freestream conditions
s	probe position

Symbols

Δ denotes difference between coefficients prop/on and prop/off, e.g. $\Delta C_Y = C_{Y_{prop/on}} - C_{Y_{prop/off}}$ at otherwise same flow conditions (α, β, U_∞)

Abbreviations

RPM revolutions per minute

I. Introduction

Since the advent of the new generation of medium-speed turboprop commuter aircraft with highly loaded propellers there has been a growing interest in and concern about the propeller slipstream aerodynamic interference effects. As the highly loaded propellers give rise to highly energetic slipstreams with high velocities the effect on e.g. the nacelles are higher than for the more conventional lightly loaded propellers. Due to propeller slipstream/-nacelle interference effects asymmetrical loads (side forces and yawing moments) could develop on an aircraft with two propellers rotating in the same direction. These effects could lead to resizing of the aircraft control surfaces and/or necessary trim changes, leading to increased drag. Therefore, the need for detailed design of the nacelles for optimum performance is more accentuated than before.

The National Swedish Board for Technical Development (STU) therefore granted FFA a research contract to carry out low speed wind tunnel investigations on these propeller slipstream aerodynamic interference effects. The major emphasis in the test was put on the physical aspect of the interference effects and the test models therefore had rather schematic layouts. The propeller, however, was one fifth scale model of the original SAAB SF-340 propeller, developed by Dowty Rotol, Ltd. UK. The model nacelles and wing were equipped with pressure holes in the slipstream washed areas.

In addition to surface pressure measurements also the propeller slipstream flowfield was surveyed by means of a traversing five hole pressure probe, resulting in distributions of velocities and pressures in the slipstream.

II. Description of Experimental Technique and Set-Up

Wind tunnel

The test was carried out in the FFA low speed wind tunnel LT1. The test section of this wind tunnel is circular with a diameter of 3.6 m. The maximum speed is about 85 m/s. However, the test described in this report was carried out in the speed range 33-61 m/s.

Wind tunnel model installation

The models were mounted in the wind tunnel by means of a tail sting arrangement (Fig. 1). The sting was mounted on a movable sting frame. The attitude of this frame (angle of attack and yaw) is controlled by means of servo motors via a strut and suspension wires.

Model-propeller-drive-unit

The propeller was driven by a hydraulic motor housed in the model nacelle. The compressed hydraulic oil was fed to the motor by a hydraulic pump situated outside the tunnel via tubes inside the sting. The hydraulic pump is power rated to about 75 kW, but the maximum propeller shaft power in this test was about 45 kW.

Model nacelle/wing

In total four different nacelle/wing combinations were tested (for geometry, see Fig. 2) both prop-off and prop-on.

The baseline nacelle was an axisymmetrical body, designed as a "minimum body" to house the hydraulic motor and with room for the sting mounting, the Scanivalves and associated plastic tubing for the pressure taps on the nacelle surface, etc. This nacelle was manufactured from a lathed wooden master in two halves made of glass fibre reinforced epoxy plastic. The two halves were screwed together along the dividing line. Inside the nacelle there were also provisions made for the proper alignment of the nacelle with the propeller axis and the sting.

For the "high" nacelle the two above-mentioned nacelle halves were separated by a cylindrical middle part. In this case the lower nacelle part was cut in the near-propeller region and here the middle part was provided with a "chin", thus forming a smoothly rounded transition region between the nacelle parts. No air inlet was simulated.

For both the nacelle layouts two unswept wing halves could be mounted. The wing had a rectangular planform with chord =0.5 m and span = 2.0 m (approx.), thus with an aspect ratio of A= 4. The airfoil section was NACA $63_{(10)}$A-012. This particular wing was chosen because it was available from earlier wind tunnel tests.

Model propeller

The four-bladed model propeller was an one-fifth scale of the original propeller of the SAAB-Fairchild SF-340 commuter aircraft (full scale diameter =126"=3.20 m). This 0.64 m diameter model propeller has been used before in the wind tunnel development work of the SF-340. The metal model propeller (and the full scale propeller made of composite materials) was designed and manufactured by the British firm Dowty Rotol, Ltd. at Glouchester, U.K. The propeller is thought to be a typical example of the highly-loaded propellers for the new generation of medium-speed commuter aircraft.

Model instrumentation

The propeller thrust and shaft torque were measured by means of strain-gauge elements mounted on the propeller shaft inside the spinner. Since these balance elements were rotating with the propeller, the balance signals were transmitted through a slip ring unit. The propeller RPM was measured by means of a magnetic pickup mounted on the hydraulic motor.

On the nacelle surface there were 96 or 144 pressure holes (for the axisymmetrical and the "high" nacelle, respectively) arranged in twelve axial stations. On each wing half there were 48 pressure holes. These wing pressure holes were located mainly in the regions where the propeller slipstream washes the wing surface. For the pressure scanning and measurement the Scanivalve technique was used. The Scanivalves were placed inside the nacelle and inside the wing halves.

The locations of the pressure taps on the nacelle and the wing are given in Figures 3 and 4 respectively.

Five-hole pressure probe

The propeller slipstream flow field was surveyed by means of a traversing five-hole pressure probe. The probe was mounted on a long stiff arm with a cranked forward part. The arm was in turn mounted on a traversing mechanism capable of radial traversing. The mechanism was firmly attached to the tail sting. The radial displacement of the probe was carried out by means of an electrical motor and was sensed by a potentiometer.

The axial and azimuthal position of the traversing mechanism could be changed by sliding and rotating it on the tail sting. The axial position of the probe could also be changed by sliding the probe arm on the traversing mechanism. The probe pressures were measured by means of five individual pressure transducers (of semiconductor type) located on the traversing mechanism. The pressure tubes were drawn in the arm.

The traversing probe arrangement and also the probe shape and dimensions are depicted in Fig. 5.

Data acquisition and presentation

During the wind tunnel runs the electrical signals from the Scanivalve pressure transducers and the propeller balance signals were multiplexed, A/D converted and then stored in the wind tunnel minicomputer (VAX 11/750). Of course, also the wind tunnel speed and propeller RPM were recorded. Each pressure value obtained constitutes an average of about 60 instantaneous values during about 860 milliseconds. This reduces the effect of random errors.

In the subsequent data analysis the nacelle and wing surface pressures were non-dimensionalized to pressure coefficients: $C_p=(p-p_\infty)/q_\infty$. The nacelle C_p's were then plotted as vectors perpendicularly to the surface. This was done at the twelve axial stations along the nacelle. For the wing both chordwise and spanwise pressure distributions were plotted.

The pressure distributions on the nacelle surface were also integrated in order to give the total loads acting on the surface. Here simple numerical Simpson double integration was performed.

The definitions of coordinate axes and forces/moments are given in Fig. 6.

In the slipstream flow field survey the 5 probe pressures and probe radial position were sensed, multiplexed, A/D converted and stored in the computer. About 350 radial positions were scanned in each run, beginning near the nacelle surface and ending at about 1.6 times the propeller radius. The radial resolution was about 1 mm.

The obtained pressure data were then converted to total slipstream speed and flow angles, total and static pressure by means of prestored probe calibration data.

III. Scope of Test

As mentioned above four configurations were tested:

Configuration	Nacelle	Wing	Propeller
CONF1	Axisymmetrical	Off	On/Off
CONF2	Axisymmetrical	On(mid-)	On/Off
CONF3	"High"	Off	On/Off
CONF4	"High"	On(low-)	On/Off

The configurations were tested at different angles of attack and yaw combinations at thrust coefficients ranging from C_F=0.05 to 0.57.

At each test point (α, β, $\beta_{.75}$, C_F, U_∞) the nacelle surface (and wing surface) pressures were measured.

For configurations 1, 2 and 4 limited propeller slipstream flow field surveys were carried out. For the selected configurations the propeller operating conditions were the same as for the surface pressure tests.

IV. Results and Discussion

Nacelle surface pressure distributions

Positive pressure coefficients C_p are plotted with arrows pointing to the nacelle surface and negative C_p from the nacelle surface. This means that the arrows indicate the directions of the pressure forces on the nacelle.

Axisymmetrical nacelle (wing-off): CONF1

Figures 7a,b depict the nacelle surface pressure distributions at $\alpha=0^{\circ}$ and 10°, respectively. The pressure distributions are shown in twelve axial stations of the nacelle, looking upstream. Propeller rotation direction is clockwise looking upstream. As can be seen for $\alpha=0^{\circ}$ (Fig. 7a) the pressure distributions are roughly circular in shape, which is expected for this axisymmetrical nacelle shape and the axisymmetrical flow conditions. There are, however, some minor deviations from the circular shape due to e.g. pressure hole imperfections (burrs).

In the near-propeller stations the pressure is higher than the ambient pressure ($C_p>0$), which, of course, is a manifestation of the pressures induced by the propeller and that constitutes the propeller thrust. As the nacelle diameter increases in the downstream direction the pressures are decreasing up to about the station where the maximum nacelle diameter occurs. Further downstream, the pressure again increases.

For $\alpha=10^{\circ}$ (Fig. 7b) the pressure distributions deviate markedly from the corresponding distributions at $\alpha=0^{\circ}$. One can observe that the pressure is higher on the right hand half of the nacelle than on the left hand half (looking upstream), thereby resulting in a side force directed to the left. In Fig. 7b also the sectional resultants of the pressure are shown as vectors (in arbitrary units).

As is seen these vectors all point to the left, giving the afore-mentioned total side force resultant. One can also note that the vectors are turned from a left-upward direction at the near-propeller stations to a left-downward direction at the most downstream stations of the nacelle. This behaviour, in combination with the magnitudes of the vectors, gives a very small resultant normal force (that is, the force in the z-direction).

The physical cause of this generation of side forces (and yawing moments) is thought to be the following: When the right-going propeller is set at a positive angle of attack, the down-going blades (at the right-hand side of the propeller disk, looking upstream) experience an increased effective blade angle and an increased resultant flow velocity and therefore an increased lift force = thrust. For the up-going blades there is a corresponding decrease in thrust due to a lower effective blade angle and a lower resultant flow velocity. The propeller thrust manifests itself in the slipstream as increased slipstream pressure (compared to the ambient pressure). Since, in average, there is higher thrust on the right hand side of the propeller disk than on the left hand side, there should be also in average a higher pressure in the right hand half on the slipstream than on the left hand half. When this non-uniform slipstream washes the nacelle downstream the propeller a pressure difference between the right and left hand halves of the nacelle is set up.

Axisymmetrical nacelle (wing-on): CONF2

The pressure distributions for this configuration clearly show the marked influence of the wing on the nacelle pressure. The wing has a straightening effect on the flow (a "turning vane" effect) (Figures 8a,b). This means that the nacelle pressure distributions at the wing stations are more symmetrical about the vertical axis than the corresponding pressure distributions without the wing. At angle of attack there is, however, still a resulting total side force to the left acting on the nacelle.

By comparing the pressure distributions for the axisymmercal nacelle wing-on/wing-off (Figures 8b and 7b, respectively) one can see that the pressure distributions close to the propeller are rather uneffected by the pressure of the wing. However, for the stations nearer to the wing the influence of the wing on the pressure distributions grows significantly.

High nacelle (wing-off): CONF3

For this non-axisymmetrical (high) nacelle (wing-off) the pressure distributions (Figures 9a,b) for the near-propeller stations are markedly asymmetrical even for $\alpha=0^{\circ}$, in contrast to the case of the axisymmetrical nacelle at $\alpha=0^{\circ}$. The pressure force resultants are concentrated to the upstream half of the nacelle. This is interpreted so that the nacelle in itself acts like a turning vane, i.e. the flow is straightened out along the nacelle.

The pressure distributions described thus result in a non-zero side force and a non-zero yawing moment at $\alpha=0^{\circ}$.

High nacelle (wing-on): CONF4

Also in this case the presence of the wing has a marked effect on the pressure distributions on the nacelle surface (Figures 10a,b). In the near-propeller region (Stations 1 and 2, say) the pressure distributions ($\alpha=0^{\circ}$ and 10°) seem rather uneffected by the wing but further downstream the influence grows quickly.

Similar to the axisymmetrical nacelle with wing (CONF2) the pressure distributions on the nacelle in the wing region become rather symmetrical about the vertical axis (due to the "turning vane" effect of the wing), which means that side force contributions from the nacelle pressures in this area are diminished.

Wing surface pressure distributions

Figures 11 and 12 show the wing surface pressure distributions for the configurations CONF2 and CONF4 at the same conditions as for corresponding nacelle surface pressure distributions already shown. In the figures also estimated "carry-over" loads over the nacelle are presented. The nacelle C_p's are projected on the wing centre plane.

Spanwise distribution of wing surface pressures (CONF2)

The figures (11a,b) clearly show the asymmetrically developed lift forces on the wing halves due to slipstream swirl. For $\alpha=0^o$ the lift forces on the wing are oppositely directed on the two wing halves. For $\alpha=10^o$ the lift forces are positive (on both the wing halves), but for both $\alpha=0^o$ and 10^o there is a resulting positive rolling moment. On the left wing leading edge there is a rather low C_p (about -8) for this case.

As also can be seen the effect of the slipstream swirl diminishes downstream the wing.

Spanwise distribution of wing surface pressures (CONF4)

These figures (12a,b) show the spanwise distribution of wing pressures for the high nacelle (low wing location). The general picture of these distributions are similar to the case with axisymmetrical nacelle with mid wing location. However, the flow around the leading edge of the port wing does not seem to be quite as large with the high nacelle/low wing combination as with the axisymmetrical nacelle/midwing combination at same angle of attack. Maybe this could partly be explained as a "turning vane" effect of the high nacelle itself, but also as an effect of the low wing location since the wing is differently located in the slipstream in this case.

Nacelle total forces and moments

The nacelle surface pressure distributions were integrated (by means of simple numerical Simpson double integration procedure) over the nacelle surfaces to give total loads acting on the nacelle. The integrations were carried out, of course, only on the nacelle surface from Stations 1 to 12, and did not incorporate e.g. the spinner. Obviously, only pressure drag due to nacelle surface normal pressures is obtained in this way. To measure the total nacelle drag one has to use a balance in order to include the viscous forces.

Total forces and moments vs. α (CONF1)

Figure 13 shows the total loads, acting on the axisymmetrical nacelle as functions of angle of attack. The loads are presented as coefficients. As is seen in the figure, and which is already indicated from the pressure distributions, there is a negative side force and a negative yawing moment on the nacelle at angles of attack. Both C_Y and C_n seem to have an approximately linear rate of decrease with increasing α. This is thought to be an effect entirely of the propeller slipstream. (In the figure the broken lines show the total loads for the propeller off configuration.)

For this configuration the normal force (C_Z) is rather uninfluenced by α. The pitching moment slope (C_{m_α}) is positive, that is, there is a negative contribution from the nacelle to longitudinal stability. As can be seen there is a slight destabilizing slipstream influence on the pitching moment. This behaviour of the normal force and the pitching moment can be seen as a verification of the slender body approximation. For a slender body at incidence there is only a force couple acting on the body, thus resulting in zero normal force and a nose-up pitching moment. The slightly larger C_m of the nacelle in the propeller slipstream could be interpreted as a small change of moment lever for the force couple.

In the figure a point corresponding to $\alpha=0^o$ and $\beta=10^o$ is plotted for the different components. Because of the symmetry of the nacelle, the yawing moment at $\beta=10^o$, $\alpha=0^o$ should have the same magnitude as the pitching moment at $\alpha=10^o$ and $\beta=0^o$ and as can be seen in the figure this is approximately true.

Total forces and moments vs. α (CONF2)

Figure 14 indicates that, for this configuration (axisymmetrical nacelle, wing on), the principal effect of the propeller slipstream at angles of attack is the same for side force and yawing moment as for the isolated nacelle. However, the respective rates of decrease of C_Y and C_n vs. α are modified.

This configuration (CONF2) has also been tested at different angles of yaw. As can be seen there is a rather strong slipstream effect on the pitching moment with β. By comparing C_{n_α} with C_{m_β} one finds that the magnitudes of these derivatives are about the same. One also finds that there is hardly any change of pitching moment slope C_{m_α} with angle of yaw.

Total forces and moments vs. α (CONF3)

For the high nacelle (wing off) there is a rather large negative yawing moment at $\alpha=0^{o}$ (Figure 15), as already is indicated from the nacelle surface pressure distributions. The yawing moment coefficient then decreases at an approximately constant rate with increasing α. The side force is also negative at $\alpha=0^{o}$ and decreases with increasing α.

The normal force vs. α exhibits a somewhat irregular behaviour. However, the pitching moment shows a monotonic increase with increasing α, that is, $C_{m_\alpha}>0$.

For this configuration there is also a rolling moment C_ℓ that can be attributed to the effect of the slipstream. Since the reference point for C_ℓ is situated on the propeller axis and since the nacelle surface is mainly located beneath this axis, there results a positive rolling moment slope C_{ℓ_α}.

Total forces and moments vs. α (CONF4)

Similar to the high nacelle/wing off configuration (CONF3) this configuration (CONF4: high nacelle/low wing) exhibits rather large side forces and yawing moments acting on the nacelle for $\alpha=0^{o}$ (Fig. 16). The magnitudes of C_Y and C_n are even higher than for the isolated high nacelle. The rate of decrease of C_Y for increasing α is about the same as for CONF3, but the rate of decrease for C_n is higher for CONF4 (that is, with the wing on).

Also, there is slightly higher C_{m_α} due to the presence of the wing.

The rolling moment C_ℓ exhibits about the same behaviour as for wing/off.

Slipstream effects on nacelle forces and moments

In order to directly estimate the propeller slipstream effects on nacelle total forces and moments, the results obtained in prop/off tests were subtracted from the corresponding prop/on results (at same freestream speed, α and β).

Effect of angle of attack

Figure 17 depicts the nacelle total forces and moments due to the presence of the propeller slipstream for the four configurations (at $\beta=0^{o}$) as functions of angle of attack. As previously has been indicated there is a monotonic decrease of the side forces and yawing moments with increasing α. For the non-axisymmetrical configurations at $\alpha=0^{o}$ both the side force and yawing moment are negative.

For the non-axisymmetrical configurations there is also a rolling moment acting on the nacelle, whereas for the axisymmetrical nacelle the rolling moment is negligible (there is no moment lever for the pressure forces).

For the axisymmetrical configurations (wing on/off) the influence of the slipstream is rather small on the nacelle normal forces and pitching moments. For the non-axisymmetrical nacelle the behaviour of the normal forces is slightly irregular. Perhaps this could be explained in terms of the above-mentioned slender body theory: Ideally the normal force for a slender body at incidence is zero; however, in real fluid flows there are also viscous effects that could disturb the balance of surface pressure forces (e.g. at least locally there could exist separated areas on the body), resulting in non-zero normal forces.

For the high nacelles there are nose-down pitching moments at $\alpha=0^{o}$. The slope of the pitching moments are positive ($C_{m_\alpha}>0$), which means that there is a negative contribution to longitudinal stability induced by the slipstream.

As can be seen there is also a propeller slipstream induced increase of the tangential forces acting on the nacelle hull, resulting in an increase of the nacelle pressure drag. These tangential forces are rather insensitive to α, for all the nacelle/wing combinations. However, one ought to remark that the above-mentioned slipstream induced pressure drag increments are only pertaining to the nacelle surfaces that are equipped with pressure taps. One should also include in the total slipstream induced nacelle pressure drag increments the surfaces of the nacelle which are not covered by the present investigations, e.g. propeller spinner and the nacelle base area.

Effect of angle of yaw

Figure 18 depicts the propeller slipstream induced nacelle forces and moments as function of angle of yaw at $\alpha=0^{o}$ for the four configurations.

For the axisymmetrical nacelle the effect of the slipstream at different β is small on the side force and the yawing moment. This corresponds, of course, to the effect of the slipstream at different α on the normal force and pitching moment of this axisymmetrical nacelle.

For the non-axisymmetrical nacelle (wing off/on) the rates of decrease for ΔC_Y and ΔC_n vs. β are less than the rates of decrease for ΔC_Y and ΔC_n vs. α, that is:

$$\left|\frac{\partial}{\partial\beta}(\Delta C_Y)\right|<\left|\frac{\partial}{\partial\alpha}(\Delta C_Y)\right|;\quad \left|\frac{\partial}{\partial\beta}(\Delta C_n)\right|<\left|\frac{\partial}{\partial\alpha}(\Delta C_n)\right|,$$

respectively.

The yawed propeller produces a slipstream where the pressure is higher on the top of the nacelle than on the lower side of the nacelle. If the nacelle were axisymmetrical this would not create any side forces or yawing moments on the nacelle. However, for the non-axisymmetrical nacelles, due to the slipstream swirl, there are different conditions for the slipstream on the left hand and right hand side of the nacelle, because of the asymmetrical location of the nacelle in the slipstream flow field.

Effect of propeller thrust coefficient C_F

As can be seen in Fig. 19, there is a monotonic propeller slipstream induced decrease of both nacelle side force and yawing moment coefficients, that is, the magnitudes are monotonically growing with increasing thrust coefficients C_F for all tested configurations (at $\alpha=5^o, \beta=0^o$). This seems logical since the thrust coefficient $C_F=F/qS$ is a measure of the pressure forces in the slipstream in relation to the pressure forces in the freestream. The propeller thrust can be envisaged as a mean pressure difference Δp acting on the propeller disk: $F=\Delta p \cdot S_p$, where S_p= propeller disk area = $\pi/4 \cdot D^2$. If one assumes that the nacelle side force is proportional to Δp and some typical exposed nacelle surface area S_{NAC}: $Y \sim \Delta p \cdot S_{NAC} = F \cdot S_{NAC}/S_p$. Now $F = C_F \cdot qS$ which leads to:

$$C_Y = \frac{Y}{qS} \sim C_F \cdot \frac{S_{NAC}}{S_p} \sim C_F$$

Thus, in this crude estimate, the side force coefficient should be proportional to C_F (at given nacelle attitude α and β).

However, as the thrust coefficient C_F increases, the velocities in the slipstream also increase (in comparison to the freestream velocity). Also the slipstream contraction increases. This means also that the momentum in the slipstream flow increases compared to the momentum of the freestream flow. If one imagines the slipstream as a jet, this jet thus becomes "stiffer" with increasing C_F, that is the deflection of the slipstream (at a given α) decreases with increasing C_F. Consequently, the exposure of the nacelle surface to the slipstream should become more pronounced.

If the change of thrust coefficient C_F is accomplished by changing the propeller blade angle, there could also be a redistribution of slipstream pressures in the radial direction of the slipstream if the thrust loading dF/dr is changed. This would also change the pressure distribution over the slipstream washed nacelle surfaces.

The change of the nacelle normal forces vs. thrust coefficient is rather small and exhibits a somewhat irregular behaviour. It is believed that this is at least partly due to the aforementioned zero normal force postulation of the slender body theory applied to the nacelle. Also, it is believed that the somewhat irregular C_Z behaviour vs. C_F stems from the inherent inaccuracy of the nacelle surface pressure integration procedure. It is also likely that there is a loss of accuracy due to the relatively sparse distribution of pressure holes on the nacelle surface.

For the axisymmetrical nacelles (wing on/off) there seems to be a rather small effect of C_F on the pitching moment, whereas for the high nacelle (wing on/off) there is a decreasing pitching moment (i.e. increasing nose-down pitching moment) with increasing C_F. Perhaps this could be interpreted as an effect of the increased slipstream "stiffness" mentioned above. For high C_F the deflection of the slipstram will be less, leading to flows over the nacelle surfaces that are more axially directed. Thus the effective angle of attack for the nacelle will decrease with increasing C_F, leading to less nose-up pitching moment.

There is an increase of slipstream induced rolling moment with increasing thrust coefficient for the non-axisymmetrical nacelle (wing on/off). The wing interference lowers the induced rolling moment, possibly due to the "turning vane" effect of the wing.

For all the tested configurations there is a monotonic increase of the tangential force with increasing C_F, with higher rates of increase for the non-axisymmetrical nacelle.

Some results from the slipstream flow field survey

Figures 20-23 show results obtained with the five-hole pressure probe in traversing the slipstream flow field for CONF2. The probe was traversed along radial lines in two axial planes, one plane located near the propeller disk (distance = 0.045 m downstream the prop plane) and one plane located at the quarter chord station of the wing. The results shown are for constant thrust (C_F=0.23, J=0.70, $\beta_{.75}=29^o$) at $\alpha=0^o$ and 10^o.

Figure 20 shows the slipstream velocities and pressures in the near-prop location at $\alpha=0^o$. In the upper part of Fig. 20 the cross-flow velocities are shown. As one can see the cross-flow is uniform for the eight radial lines. Here the presence of the wing is hardly noticeable (the distance to the wing leading

edge is 1.22 prop radius). One can see that the slipstream has contracted about 2% of the prop radius. Outside this slipstream boundary there is not any tangential (rotational) velocity component. The slipstream boundary is also clearly identified in the middle part of Fig. 20, where the axial and radial slipstream velocity components have been plotted as vectors. The maximum axial over-velocity is about 43% of the free stream speed, occuring at about 80% prop radius. Outside the slipstream boundary the velocity is lower than the free stream speed. This is a consequence of the aerodynamic "sink" effect of the propeller.

In the lower part of Fig. 20, the corresponding static pressure coefficients are depicted. As one can see the pressure is higher than the free stream pressure ($C_p>0$) within the slipstream boundary. This is thought to be a manifestation of the propeller thrust. The propeller acts like an "actuator disk" sustaining a pressure difference across itself. Of course, the slipstream pressures also are affected by the shape of the nacelle and the presence of the wing. The C_p-distributions also clearly show the slipstream boundary by a marked decrease in C_p-value. This is explained as an effect of the blade tip vortices. Since the obtained slipstream pressures are time-averaged values (due to the inability of the pressure probe to measure instantaneous pressures) the values of C_p in the vicinity of the slipstream boundary are uncertain. Outside the boundary one can see that $C_p>0$, indicating a speed lower than the freestream speed.

Figure 21 shows the corresponding quanties at $\alpha=10^0$ in the near-prop plane. Here one can notice how the distributions of the cross flow velocities are markedly asymmetrical. The slipstream boundary is no longer concentric with the prop axis, but has been displaced upwards. Outside the slipstream boundary there is a superimposed vertical velocity field due to angle of attack. This "upwash" is also thought to be affected by the induced circulation on the two wing halves, but to a lesser extent.

The slipstream pressure distributions for $\alpha=10^0$ also clearly indicate the upward displacement of the slipstream boundary. When the propeller is inclined to the freestream, the downgoing blade (at the right hand side of the disk, looking upstream) experiences a higher effective blade angle, thereby creating a higher thrust leading to higher pressure in the slipstream. This is clearly visible for e.g. radius (1) in Fig. 21 (cf corresponding radius in Fig. 20). As indicated before the nacelle surface pressures are higher in the right hand side of the nacelle (see Fig. 7b).

Figures 22 and 23 depict the corresponding slipstream flow patterns for a probe traversing plane located at the wing quarter chord station. Here the probe was traversed along lines at constant height above and below the wing (about 3 mm height). Due to the presence of the wing there is a considerable change of the flow pattern. For $\alpha=0^0$ (Fig. 22) the cross flow velocities no longer are symmetrical. However, due to the geometrical symmetry the cross flow velocities seem to be antisymmetrical along radial lines displaced 180^0 to each other. For the wing the corresponding lines are: right wing upper side – left wing lower side and right wing lower side – left wing upper side. The slipstream boundary shape is also considerably influenced by the wing. On the upper side of the right wing the boundary is displaced outwards and on the lower side it displaced inwards. Near to the nacelle surface tangential velocities are directed oppositely to the propeller swirl (Fig. 22).

For $\alpha=10^0$, the abovementioned antisymmetrical flow pattern is disturbed. The slipstream boundary in this case is displaced vertically. In the symmetry plane the boundary is displaced about 10% prop radius upwards (radius (3)) and about 30% prop radius (radius (8)).

V. Concluding Remarks

A limited analysis of detailed wind tunnel investigations on different wing combinations nacelle in propeller slipstreams has shown that

- for a propeller at angle of attack the slipstream pressure field becomes asymmetrical resulting in significant side forces and yawing moments on the nacelles. The physical cause of the generation of the asymmetrical nacelle surface pressure distributions is explained by the cyclic variation of propeller blade thrust around the propeller disk. At positive angle of attack a down-going blade experiences an increased effective blade angle and thereby produces more thrust. For the up-going blade there is a corresponding decrease of thrust. For non-axisymmetrical nacelles with a asymmetrical location within the slipstream there are also non-zero side forces and yawing moments even at $\alpha=0^0$. Also for the tested non-axisymmetrical nacelles there is a positive rolling moment acting on the nacelle,

- for non-axisymmetrical nacelles there is "turning vane" effect of the nacelle itself in that the nacelle straightens out the asymmetrical pressure field induced by the slipstream for a propeller at angle of attack,

- the presence of a wing joining the nacelle has an marked influence on the detailed nacelle surface pressure distributions,
- wing surface pressure distributions show that there is a considerable flow around the wing leading edge due to slipstream swirl. The amount of flow around the leading edge is dependent of the location of the wing in the slipstream field,
- for the four investigated nacelle/wing combinations there seems to be nacelle pressure drag increments due to the slipstream. For a given thrust coefficient these pressure drag increments are rather insensitive to angle of attack and yaw,
- the propeller slipstream induced side forces and yawing moments (at zero angle of yaw) are strongly dependent on thrust coefficient C_F. This seems logical since the slipstream pressures, and thereby the nacelle surface pressures, are directly related to propeller thrust. However, it is also believed that the precise shape of the nacelle surface pressure distributions is also dependent on propeller thrust grading dT/dr, which depends on propeller type and pitch setting.

In this paper only a small portion of all the obtained experimental data is presented, but it is hoped that the results shown could be of some help in the understanding of the rather complex aerodynamic phenomena associated with propeller slipstream interference effects. For more detailed information, see References 1, 2.

VI. References

[1] Samuelsson, I. "Low Speed Wind Tunnel Investigation of Propeller Slipstream Aerodynamic Effects on Different Nacelle/Wing Combinations".
Part 1. "Total Forces and Moments and Pressure Distributions on Nacelle/Wing at Different Angles of Attack and Yaw and at Different Thrust Coefficients".
FFA TN 1987-22, 1987.

[2] Samuelsson, I. "Low Speed Wind Tunnel Investigation of Propeller Slipstream Aerodynamic Effects on Different Nacelle/Wing Combinations".
Part 2. "Propeller Slipstream Flow Surveys (3 Velocity Components and Dynamic/Total Pressures) at Different Angles of Attack/Yaw and at Different Thrust Coefficients".
(to be published)

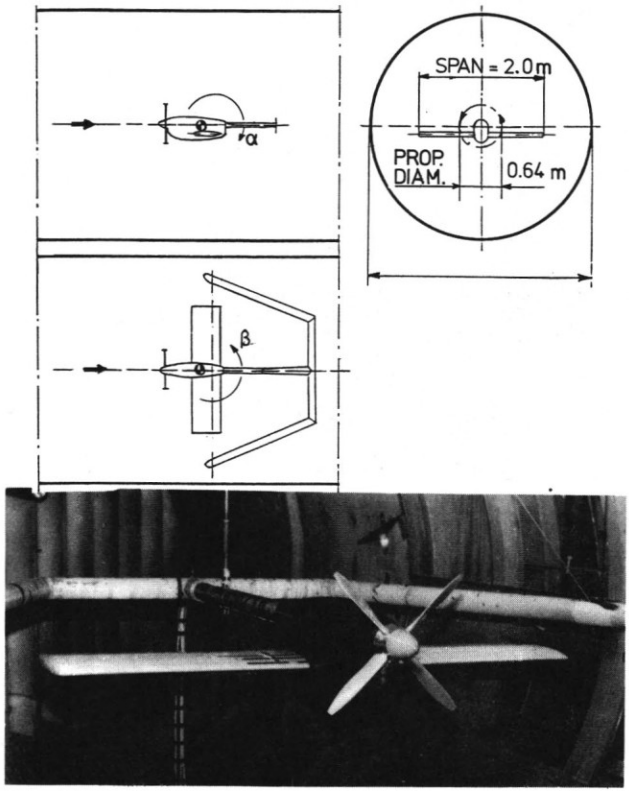

Fig. 1 Model installation in the wind tunnel

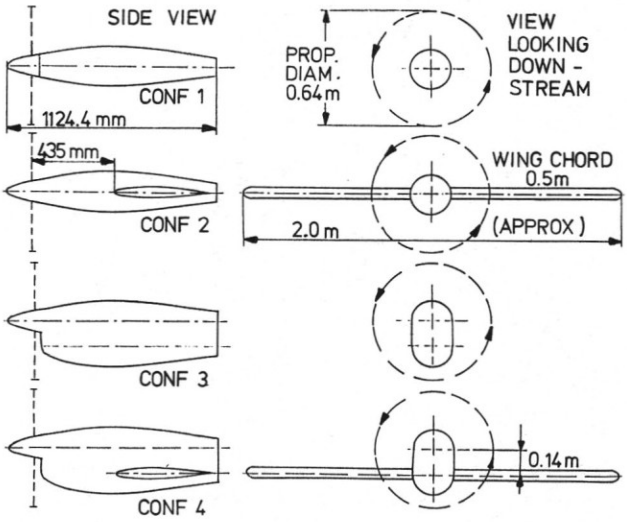

Fig. 2 Tested model nacelle/wing configurations

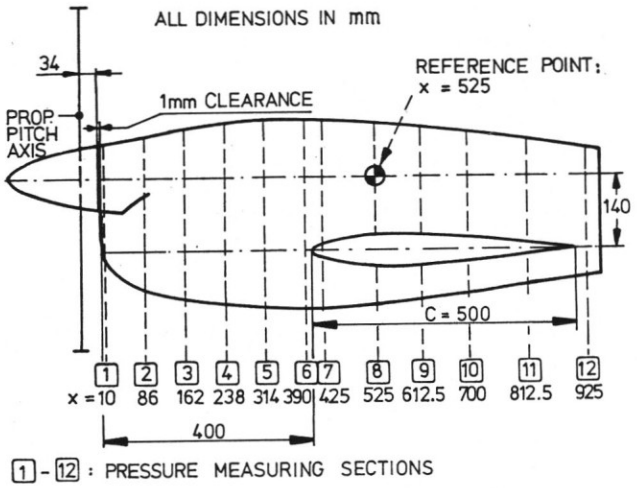

Fig. 3 Axial positions of nacelle pressure taps

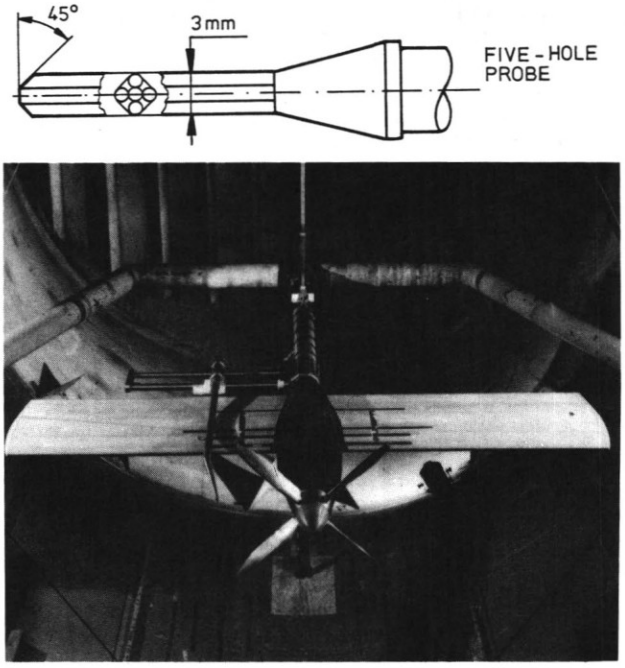

Fig. 5 Five-hole probe and probe traversing mechanism

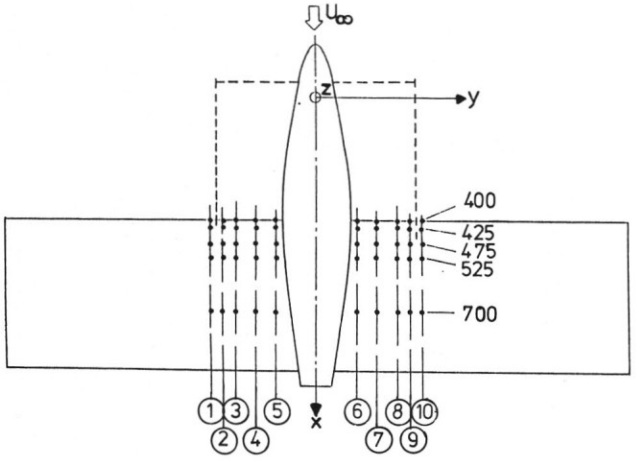

Fig. 4 Locations of wing pressure taps (upper and lower wing surfaces)

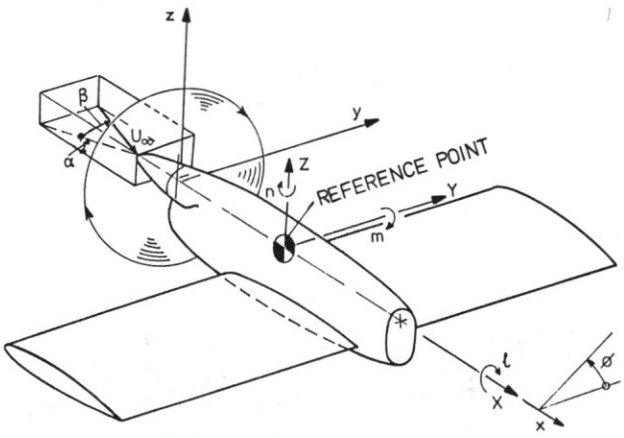

Fig. 6 Definition of coordinate system and nacelle forces and moments

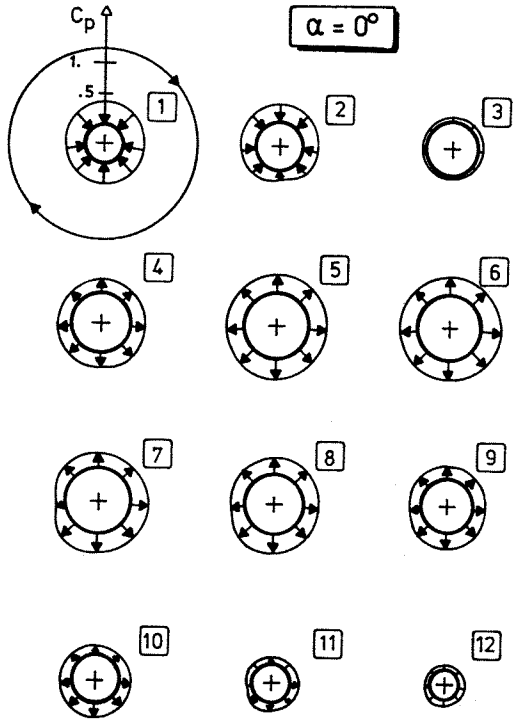

Fig. 7a Nacelle pressure distributions
(CONF1: wing-off)
U_∞=50 m/s, N=6650 rpm, $\beta_{.75}$=29°
C_F=0.23, J=0.70, α=0°, β=0°

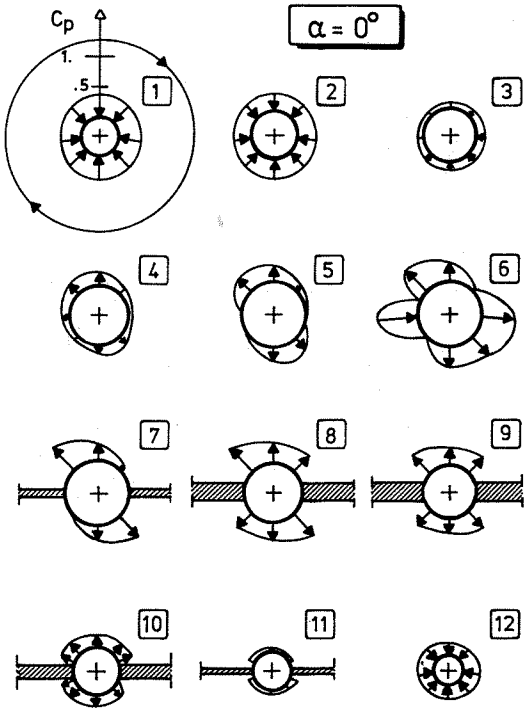

Fig. 8a Nacelle pressure distributions
(CONF2: wing-on)
U_∞=50 m/s, N=6650 rpm, $\beta_{.75}$=29°
C_F=0.23, J=0.70, α=0°, β=0°

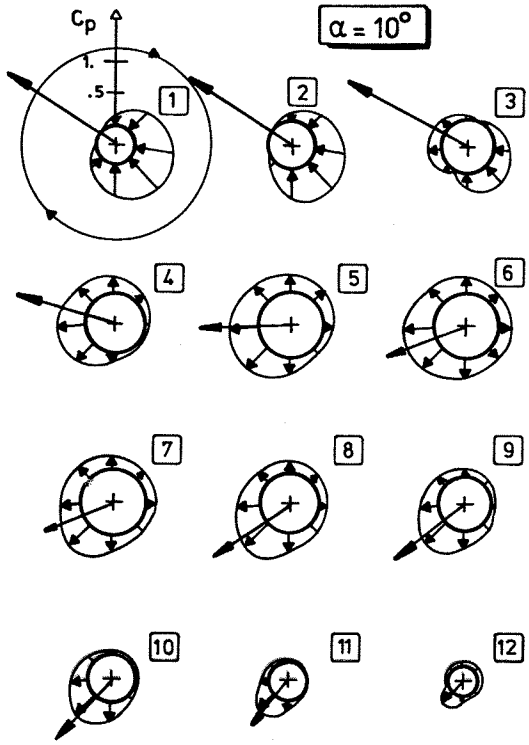

Fig. 7b Nacelle pressure distributions
(CONF1: wing-off)
U_∞=50 m/s, N=6650 rpm, $\beta_{.75}$=29°
C_F=0.23, J=0.70, α=10°, β=0°

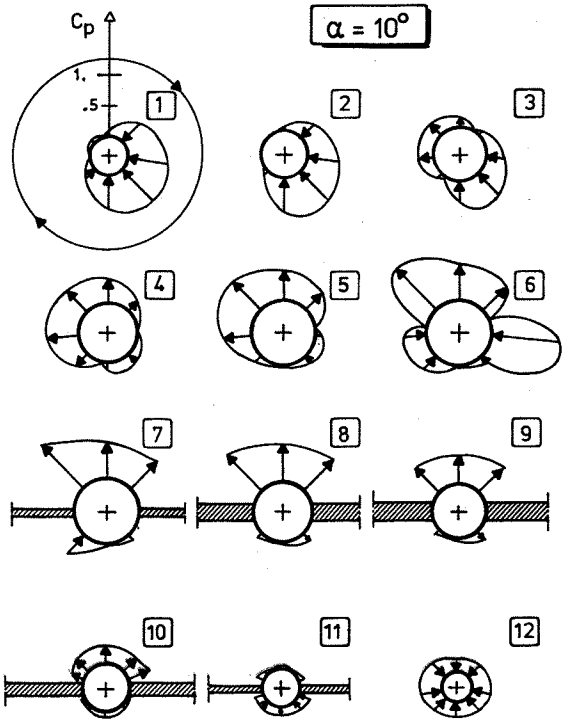

Fig. 8b Nacelle pressure distributions
(CONF2: wing-on)
U_∞=50 m/s, N=6650 rpm, $\beta_{.75}$=29°
C_F=0.23, J=0.70, α=10°, β=0°

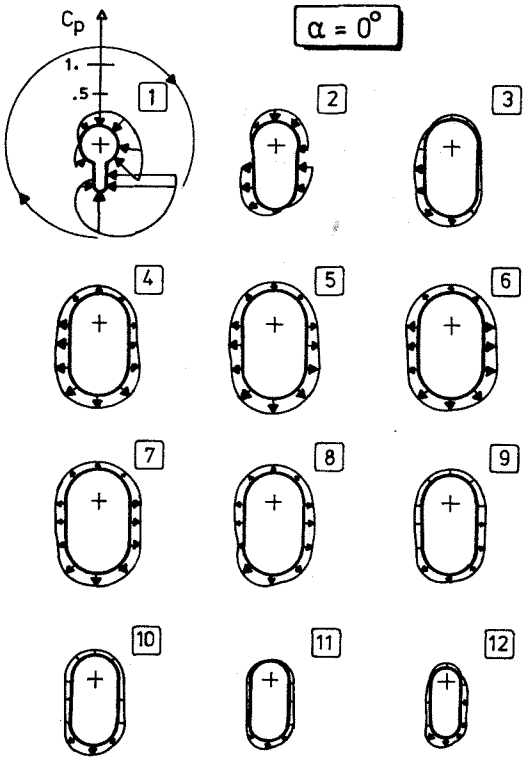

Fig. 9a Nacelle pressure distributions
(CONF3: wing-off)
U_∞=50 m/s, N=6650 rpm, $\beta_{.75}$=29°
C_F=0.23, J=0.70, α=0°, β=0°

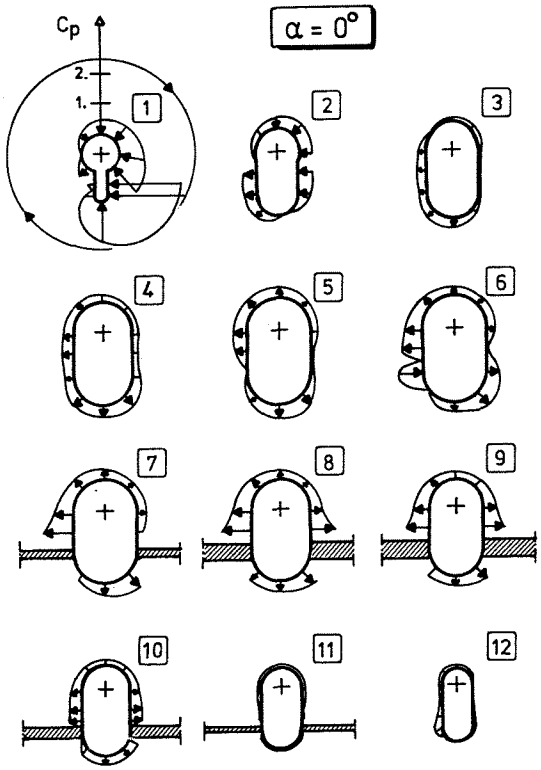

Fig. 10a Nacelle pressure distributions
(CONF4: wing-on)
U_∞=50 m/s, N=6650 rpm, $\beta_{.75}$=29°
C_F=0.23, J=0.70, α=0°, β=0°

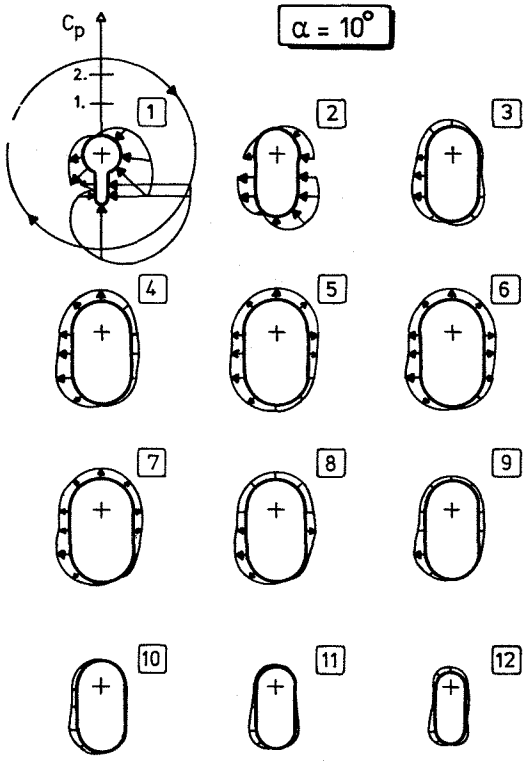

Fig. 9b Nacelle pressure distributions
(CONF3: wing-off)
U_∞=50 m/s, N=6650 rpm, $\beta_{.75}$=29°
C_F=0.23, J=0.70, α=10°, β=0°

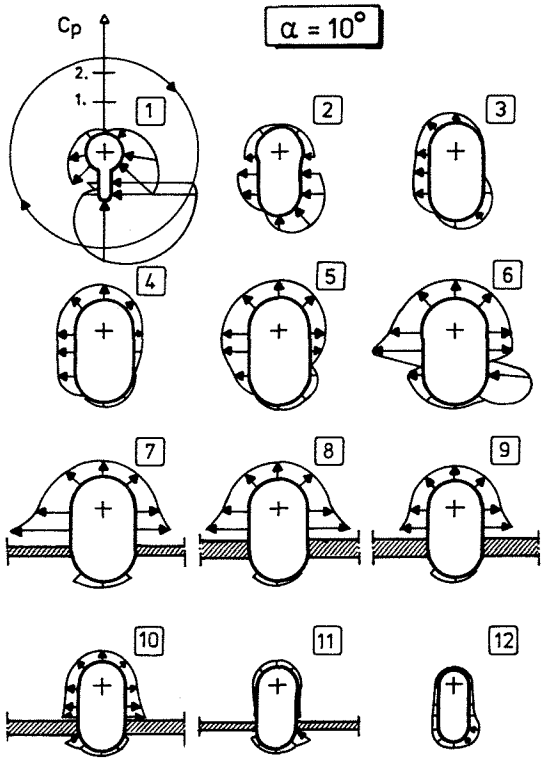

Fig. 10b Nacelle pressure distributions
(CONF4: wing-on)
U_∞=50 m/s, N=6650 rpm, $\beta_{.75}$=29°
C_F=0.23, J=0.70, α=10°, β=0°

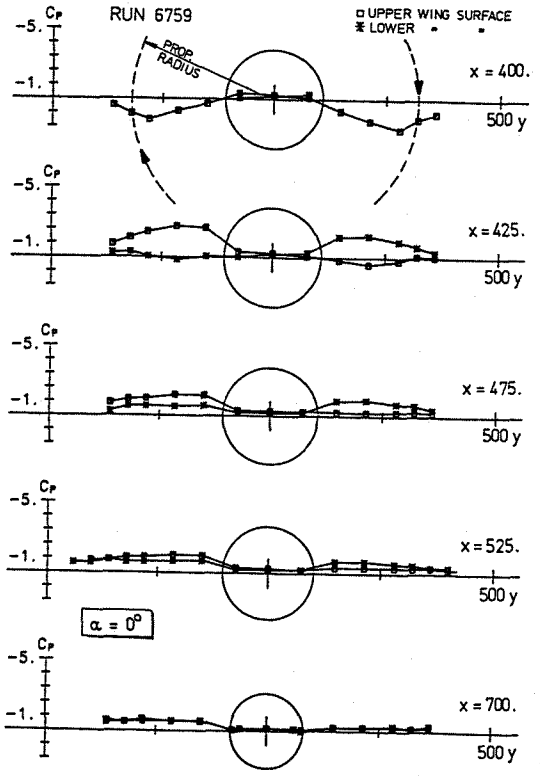

Fig. 11a Spanwise wing surface pressure distributions (CONF2)
U_∞=50 m/s, N=6650 rpm, $\beta_{.75}$=29°
C_F=0.23, J=0.70, α=0°, β=0°

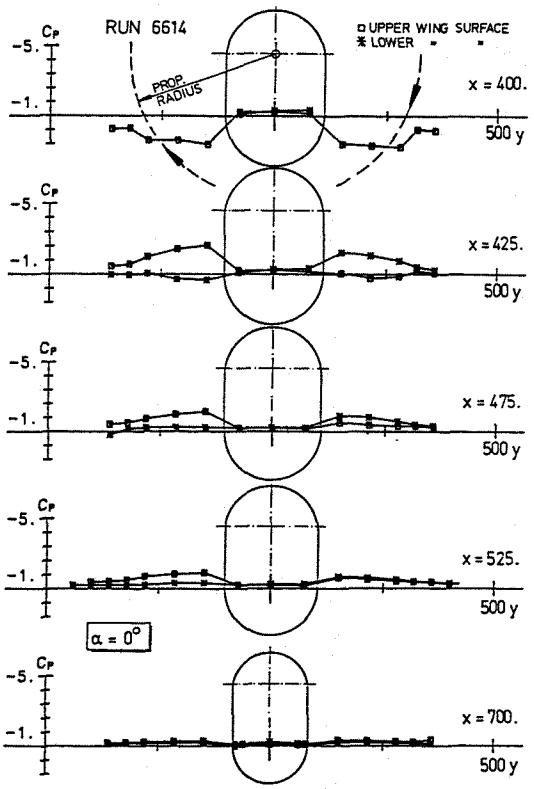

Fig. 12a Spanwise wing surface pressure distributions (CONF4)
U_∞=50 m/s, N=6650 rpm, $\beta_{.75}$=29°
C_F=0.23, J=0.70, α=0°, β=0°

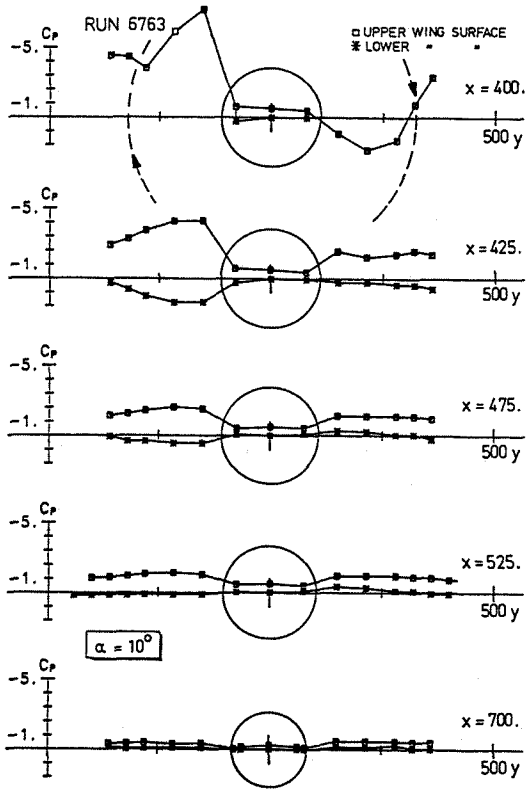

Fig. 11b Spanwise wing surface pressure distributions (CONF2)
U_∞=50 m/s, N=6650 rpm, $\beta_{.75}$=29°
C_F=0.23, J=0.70, α=10°, β=0°

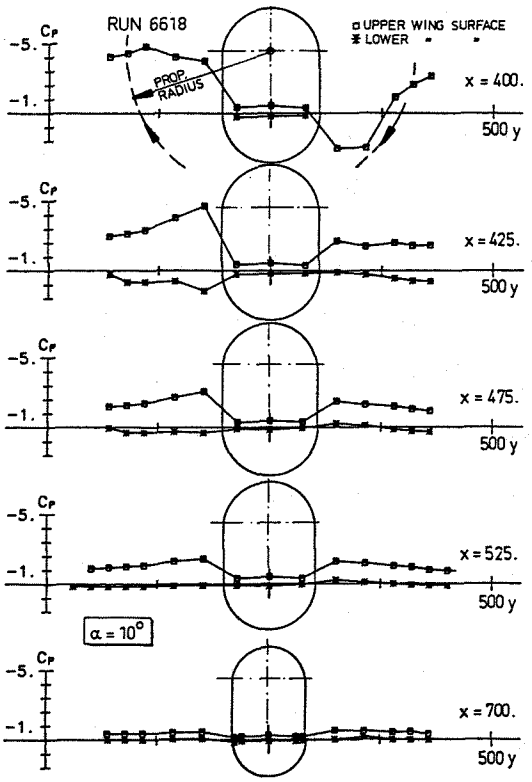

Fig. 12b Spanwise wing surface pressure distributions (CONF4)
U_∞=50 m/s, N=6650 rpm, $\beta_{.75}$=29°
C_F=0.23, J=0.70, α=10°, β=0°

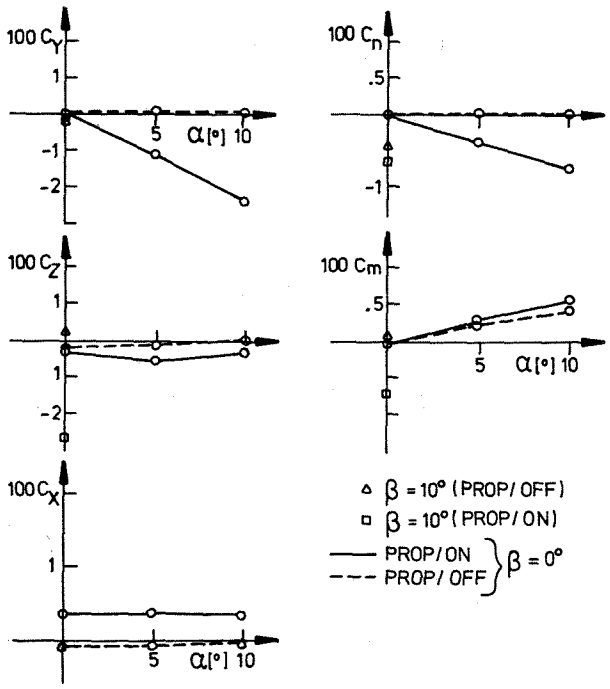

Fig. 13 Nacelle total forces and moments vs. α (CONF1: wing/off)
U_∞=50 m/s, N=6650 rpm, $\beta_{.75}$=29°
C_F=0.23, J=0.70, β=0°

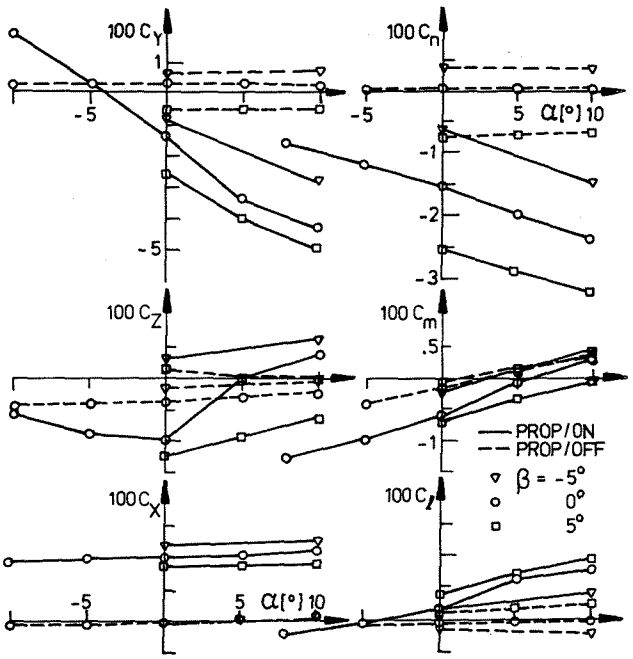

Fig. 15 Nacelle total forces and moments vs. α (CONF3: wing/off)
U_∞=50 m/s, N=6650 rpm, $\beta_{.75}$=29°
C_F=0.23, J=0.70, β=0°

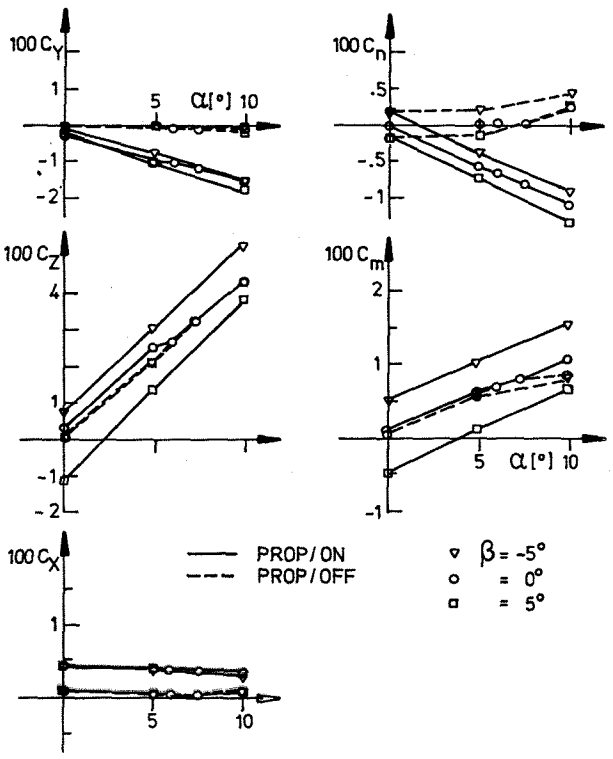

Fig. 14 Nacelle total forces and moments vs. α (CONF2: wing/on)
U_∞=50 m/s, N=6650 rpm, $\beta_{.75}$=29°
C_F=0.23, J=0.70, β=0°

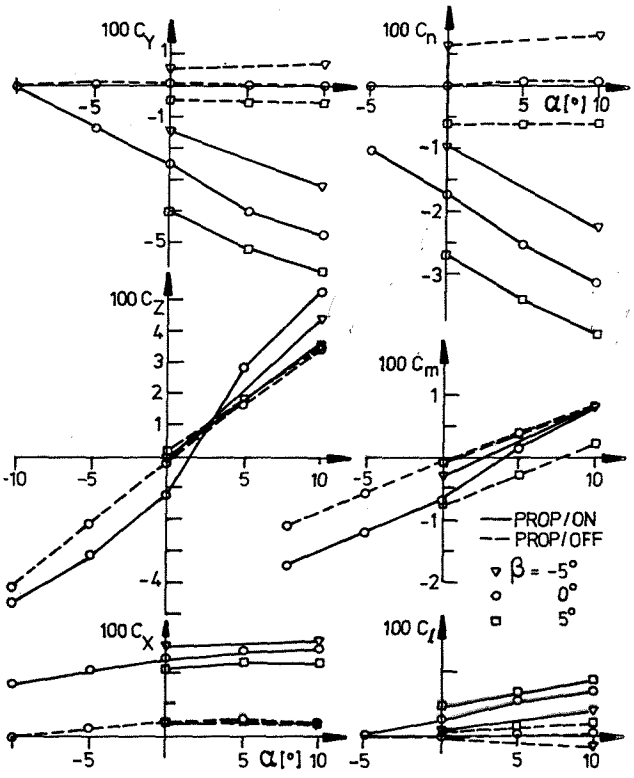

Fig. 16 Nacelle total forces and moments vs. α (CONF4: wing/off)
U_∞=50 m/s, N=6650 rpm, $\beta_{.75}$=29°
C_F=0.23, J=0.70, β=0°

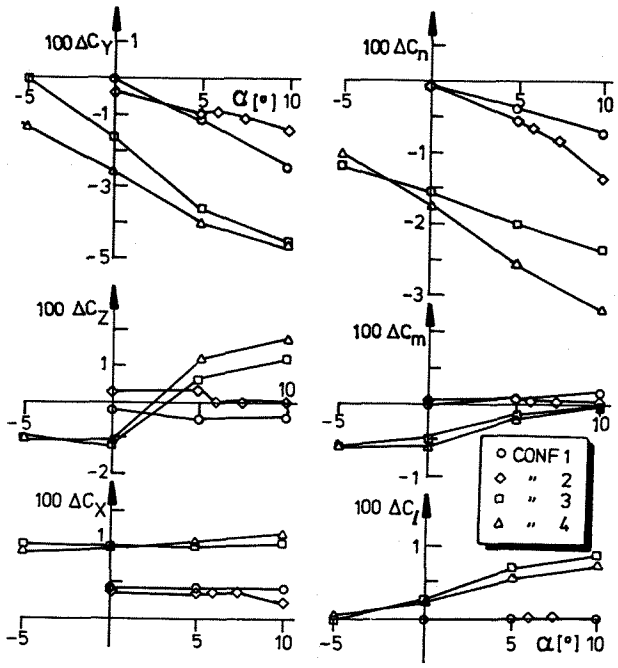

Fig. 17 Slipstream effects on nacelle total forces and moments. Effect of angle of attack.
U_∞=50 m/s, N=6650 rpm, $\beta_{.75}$=29°
C_F=0.23, J=0.70, β=0°

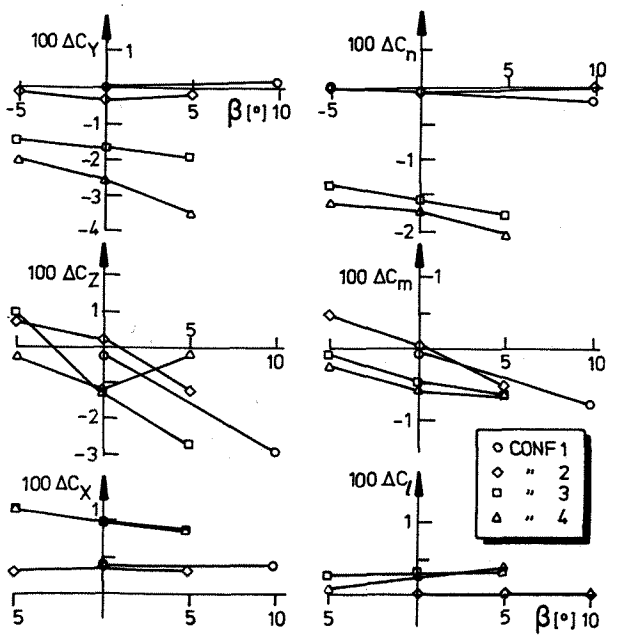

Fig. 18 Slipstream effects on nacelle total forces and moments. Effect of angle of yaw.
U_∞=50 m/s, N=6650 rpm, $\beta_{.75}$=29°
C_F=0.23, J=0.70, α=0°

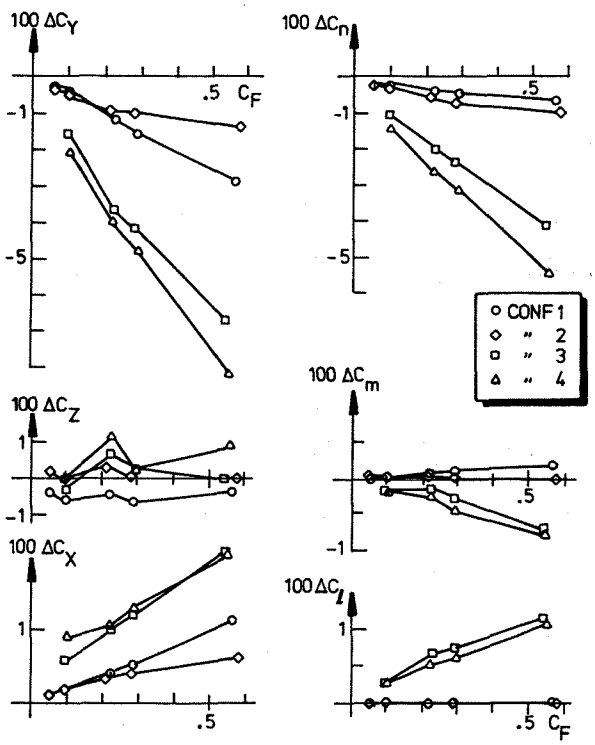

Fig. 19 Slipstream effects on nacelle total forces and moments. Effect of propeller thrust coefficient C_F.
α=5°, β=0°

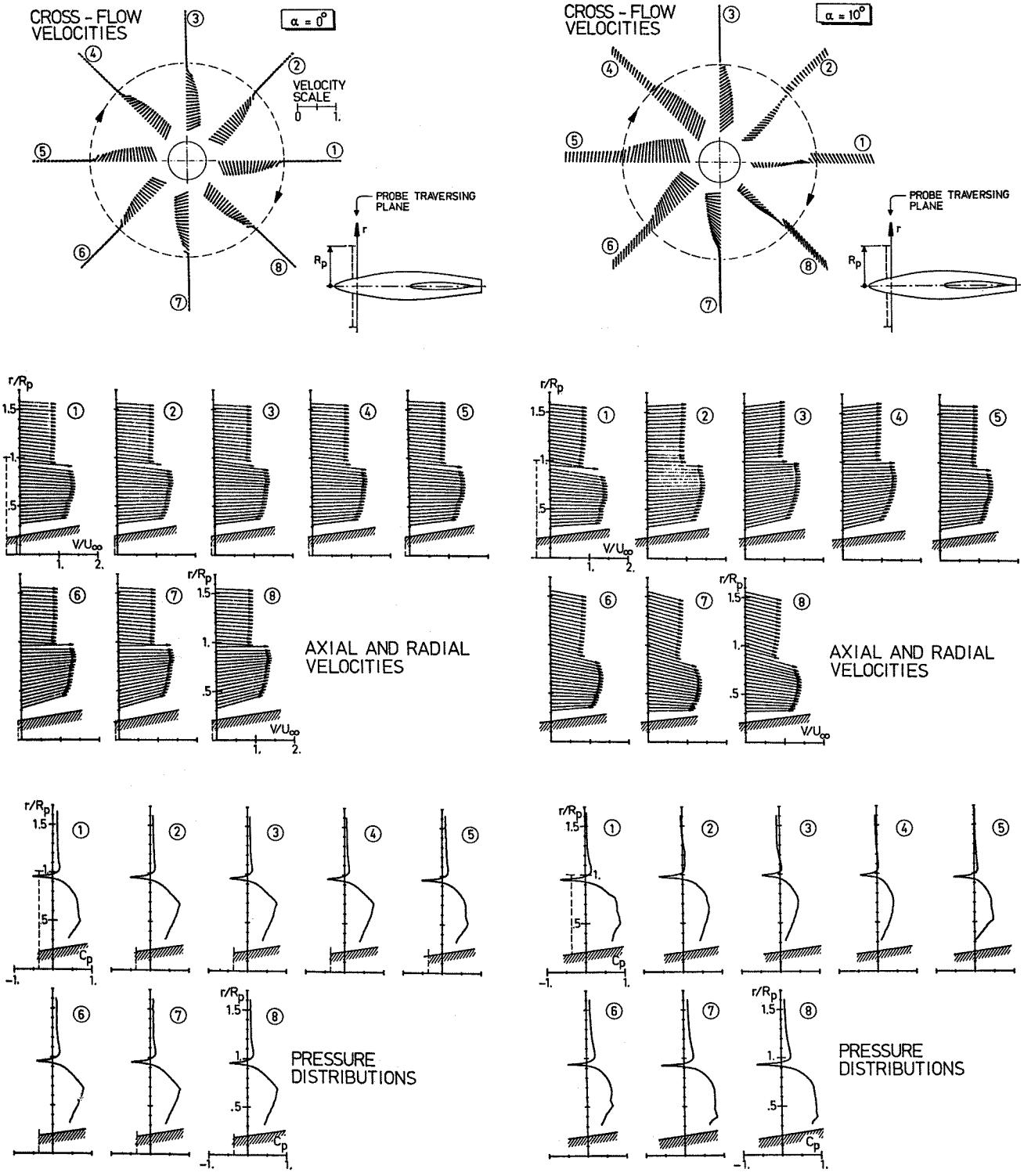

Fig. 20 Slipstream flow field survey Velocities and pressures along radial lines. CONF2. Probe traversing plane x=0.045 m downstream prop disk
U_∞=50 m/s, N=6650 rpm, $\beta_{.75}$=29°
C_F=0.23, J=0.70, α=0°, β=0°

Fig. 21 Slipstream flow field survey Velocities and pressures along radial lines. CONF2. Probe traversing plane x=0.045 m downstream prop disk
U_∞=50 m/s, N=6650 rpm, $\beta_{.75}$=29°
C_F=0.23, J=0.70, α=10°, β=0°

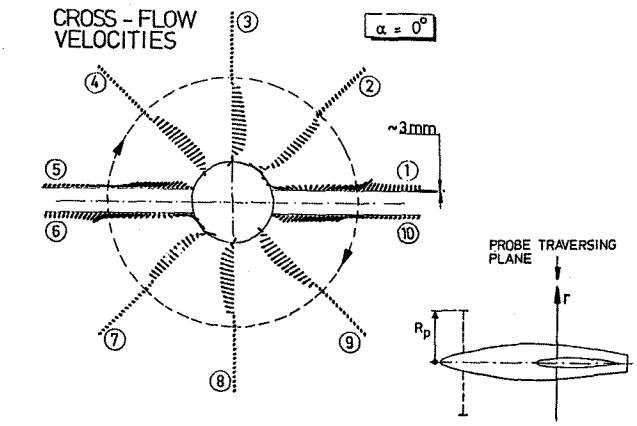

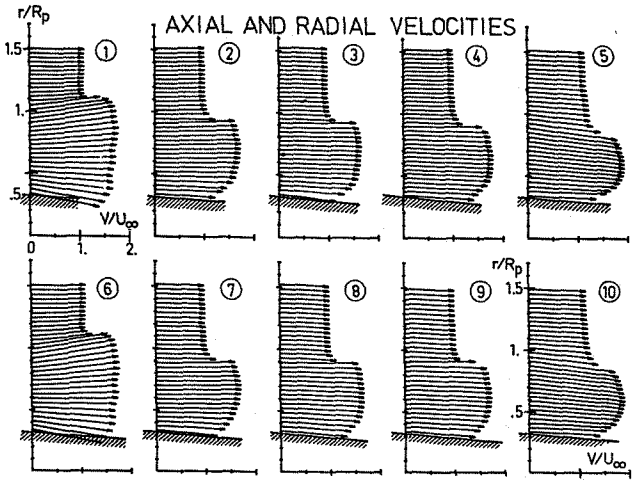

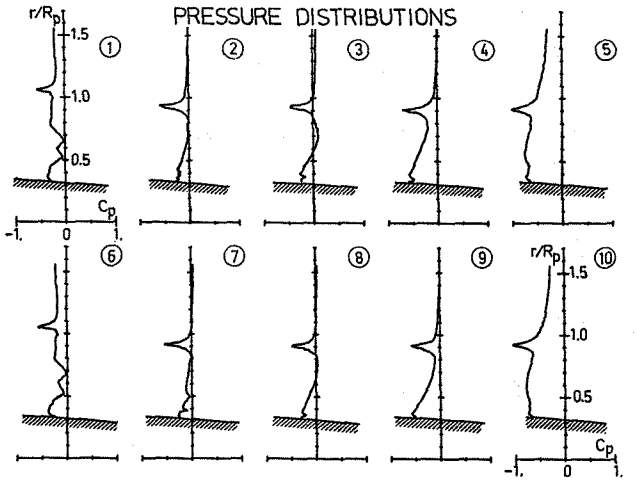

Fig. 22 Slipstream flow field survey Velocities and pressure, CONF2. Probe traversing plane x=0.560 m downstream prop disk (at wing quarter chord station)
U_∞=50 m/s, N=6650 rpm, $\beta_{.75}$=29°
C_F=0.23, J=0.70, α=0°, β=0°

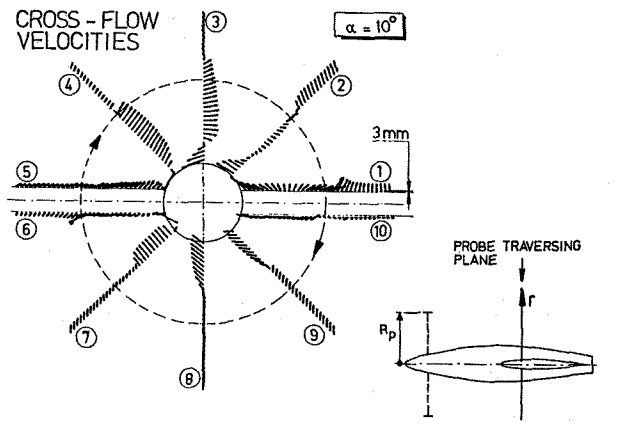

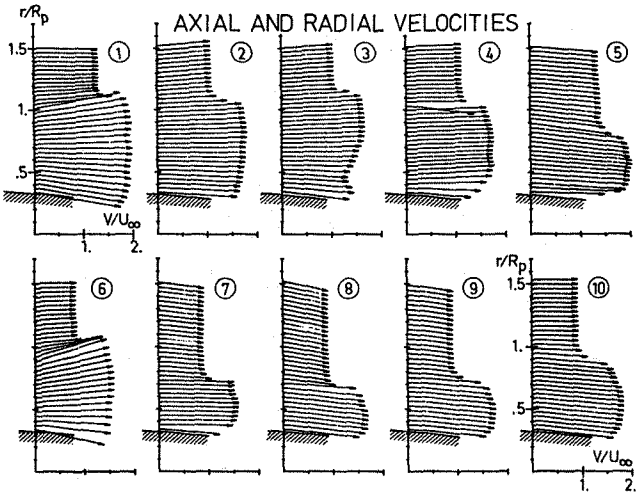

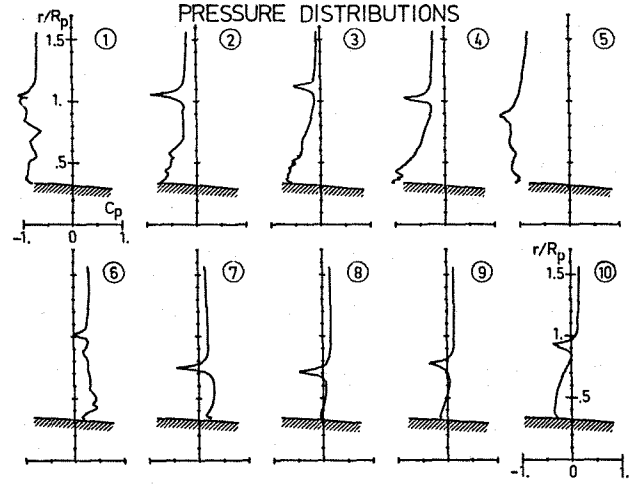

Fig. 23 Slipstream flow field survey Velocities and pressure, CONF2. Probe traversing plane x=0.560 m downstream prop disk (at wing quarter chord station)
U_∞=50 m/s, N=6650 rpm, $\beta_{.75}$=29°
C_F=0.23, J=0.70, α=10°, β=0°